RSC Advances

PAPER

View Article Online
View Journal | View Issue

Cite this: *RSC Adv.*, 2024, **14**, 35715

Piezoresistivity and strain-sensing behaviour of poly(butylene adipate-*co*-terephthalate)/multiwalled carbon nanotube nanocomposites

Kedar Nath Dhakal, [abcd] Ralf Lach, [e] Wolfgang Grellmann, [e] Beate Krause, [b] Jürgen Pionteck [b] and Rameshwar Adhikari *[acd]

Multiwalled carbon nanotubes (MWCNTs) at different concentrations, ranging from 0.5 to 10 wt%, as a conductive filler, were incorporated into poly(butylene adipate-*co*-terephthalate) (PBAT), a flexible biodegradable copolyester, *via* melt-mixing, followed by compression moulding. The electrical conductivity of the prepared nanocomposites was evaluated by considering their volume resistivity value. The volume resistivity values of the nanocomposites suggested a quite low percolation threshold between the MWCNT concentration of 0.5 and 1 wt%. The corresponding volume resistivity values of the nanocomposites in the range of $(6.90 \pm 3.16) \times 10^5$ Ω cm to $(1.24 \pm 0.41) \times 10^1$ Ω cm implied their suitability for strain-sensing applications. The change in the electrical resistance of the nanocomposites was measured simultaneously with tensile testing to evaluate their piezoresistivity. The deformation behaviour of the nanocomposites was correlated with relative resistance change ($\Delta R/R_0$) *via* a cyclic-strain test to investigate the stability of their strain-sensing behaviour. A non-linear and exponential-like increment in the $\Delta R/R_0$ values of the nanocomposites as a function of mechanical strain during tensile stretching confirmed their piezoresistivity. $\Delta R/R_0$ values fitted well with an increase in applied mechanical strain from 2% to 8% during the cyclic-strain test, which revealed the low-strain sensing potential of the nanocomposites, provided by their stable and intact microstructure formed *via* continuous stretching and releasing during the test; this was further supported by the reproducibility of the $\Delta R/R_0$ values in the cyclic-strain test with 7% applied strain in 15 cycles. Additionally, the uniformly extended net-like morphology of the nanocomposites with an entangled network of MWCNTs throughout the polymer matrix was revealed by their electron micrographs.

Received 3rd July 2024
Accepted 23rd October 2024

DOI: 10.1039/d4ra04826a

rsc.li/rsc-advances

Introduction

High-performance wearable strain sensors with multiple-location sensing capacity have diverse applications ranging from monitoring the human body to the surroundings, including human health, motion, blood pulse, breathing, finger sensing, structural variation, and sports performance, as well as in soft robotics, rehabilitation, *etc.*[1–7] Meanwhile, current technological advancements are making the lifetime of electronic gadgets shorter, leading to the global problem of e-waste.[8,9] In this case, the fabrication of degradable and environmentally compatible electronics using biodegradable and bio-based polymers is a strategy to address the problems of e-waste and plastic waste.[9–13] This has inspired scientists to develop environmentally sustainable, low-cost, light-weight, and flexible polymeric materials with anti-corrosion properties, which can be integrated into degradable electronics, addressing the above-mentioned problems.[14,15] Degradable and electrically conductive polymer composites (CPCs) with deformability and multifunctional performance are suitable materials for this purpose, which overcome the poor flexibility (rigidity) and brittleness of conventional strain sensors.[2,16–20] The soft nature and elastic stretchability of CPCs make them qualified for deformation sensing, which can be fabricated through the development of functional microstructure within them, and their properties can be tuned by altering these microstructures.[2,19–23] Multifunctional CPCs can be prepared *via* the incorporation of inherently conductive fillers such as carbon nanostructures into a flexible and elastomeric polymer matrix.[24,25] Melt-mixed CPCs that are formed through wetting the fillers by polymer melts are preferred for their outstanding carrier mobility and advanced engineering applications, which are free of filler slippage and

[a]*Central Department of Chemistry, Tribhuvan University, Kirtipur, Kathmandu, Nepal. E-mail: nepalpolymer@yahoo.com*
[b]*Leibniz-Institut für Polymerforschung Dresden e.V. (IPF), Hohe Straße 6, 01069 Dresden, Germany*
[c]*Nepal Polymer Institute (NPI), P. O. Box 24411, Kathmandu, Nepal*
[d]*Research Centre for Applied Science and Technology (RECAST), Tribhuvan University, Kathmandu, Nepal*
[e]*Polymer Service GmbH Merseburg (PSM), Geusaer Straße 81f, 06217 Merseburg, Germany*

dislocation problems in comparison to other composites, including deposited, sprayed, and sandwiched layers.[25–27] Accordingly, scientists have devoted their efforts to fabricating environment-friendly, cost-effective and high-performance strain sensors using low-cost materials used in daily life. For example, Duan *et al.* fabricated an environmentally benign strain sensor employing a facile solution casting method using carbon ink and elastic core-spun yarn.[12] Similarly, the fabrication of an eco-friendly and cost-effective pressure sensor using carbon ink and filter paper was reported by Feng *et al.*[21] Moreover, Zhang *et al.* followed a green and effective method to fabricate an ionogel-based strain sensor using carbon sponge and dextran.[4]

Piezoresistivity is the fundamental property required for CPC, by which they convert mechanical deformation (stress, strain, pressure, *etc.*) into electrical signals. Specifically, piezoresistivity is the deformation-induced change in the electrical resistance of materials, which endows them with the strain-sensing capacity of a resistive-type sensor with a simple structure, wide and convenient signal detection, and high sensitivity. The filler particles of CPC are bound by the polymer matrix, and consequently the piezoresistive properties of CPC are accompanied by a structural variation in their conductive filler network during mechanical deformation (stress, strain, stretching, bending, folding, twisting, *etc.*). This structural variation is recovered upon removal of the deformation due to the elastic recovery of the polymer matrix.[7,21,22,28,29] Destruction followed by reconstruction of the electrically conductive filler network during and after mechanical deformation, respectively, results in a synchronized resistance–strain response.[24,30,31] High elongation at break and elastic recovery of CPC after deformation are the general requirements for sensing large strain, which becomes possible in flexible and stretchable CPC.[7,28,29,32] However, a linear-type piezoresistivity plays a significant role in sensing low and subtle strain.[33]

The piezoresistive performance of CPC with low filler concentrations at which a perfect conductive network cannot be formed by the physical contact between the filler particles is interpreted by the tunnelling effect. The electrons can pass between the filler particles due to this effect (within quantum tunnelling distance) through a polymer thin layer without any conductive path. The strain-sensing behaviour of this type of CPC is based on the change in tunnelling distance between the filler particles during stretching and releasing.[28,32,34] At a higher filler concentration, the conductive network is formed by the physical contact and overlapping of the filler particles. The quantified deformation of this network as a function of mechanical strain endows CPC with piezoresistive strain sensitivity. The increased electrical resistance of these CPC during deformation is carried out by the disconnection of the filler particles.[29] The correlation between the relative resistance change ($\Delta R/R_0$) and quantified deformation is taken as the strain sensitivity of CPC, which is the basis for integrating them into strain sensors.[35]

Thermoplastic and elastomeric CPC filled with carbon nanostructures have emerged as promising candidates for deformation sensing due to their lightweight and excellent mechanical and electrical properties. Furthermore, their sensitivity can be tuned altering the concentration, dispersion, aspect ratio and geometry of the nanofillers.[15,36–38] Generally, carbon nanotubes (CNT) are the preferred conductive fillers to prepare these materials because of their outstanding electrical, thermal and mechanical properties, and high aspect ratio. CNT endow multifunctional properties to the resulting CPC due to their outstanding reinforcement effect.[7,21,39,40] Also, the high aspect ratio and curved structure of CNT result in a larger number of CNT-to-CNT contacts, due to which low CNT concentrations will be sufficient to provide electrical conductivity, leading to better mechanical properties.[25,29] Alternatively, CNT are elastic and piezoresistive in nature, which possess pressure-sensing function and can be employed as small sensors; however, the fabrication of these sensors is challenging and vulnerable from an application point of view. Therefore, they can be used as conductive fillers to prepare CPC with improved electrical, mechanical and thermal properties as suitable strain-sensing materials.[20,27,34] Hence, conductive carbon-filled deformable and flexible CPC with tuned electrical and mechanical properties can be employed as alternatives to conventional metal-based sensors due to their advantages of higher range of sensitivity (subtle to large strain) and flexibility.[41–43] Li *et al.* fabricated a high-performance and low-cost capacitive strain sensor using carbon ink-modified filter paper.[20] Yuan *et al.* prepared a high-sensitivity strain sensor using latex tube elastomers and CNT for motion detection and gesture reconstruction.[2] Similarly, Huang *et al.* fabricated an electrochemical strain sensor with wide detection range using Cu/Al electrodes and core-spun yarn coated with LiCl-CNT. Furthermore, Huang *et al.* prepared a self-powered and cost-effective pressure sensor using LiCl–CNT and Li–Cl filter papers.[1,3]

In the present study, poly(butylene adipate-*co*-terephthalate) (PBAT), an elastomeric aliphatic–aromatic biodegradable copolyester,[43,44] was employed as a deformable polymer matrix, whereas multiwalled carbon nanotubes (MWCNT) were used as conductive fillers. To date, many studies have been reported on the preparation of low-cost, lightweight and degradable composite materials using PBAT.[45–47] Furthermore, the mechanical, thermal, rheological, antibacterial and anti-static properties of PBAT/CNT nanocomposites have been investigated.[48,49] Similarly, the electrical conductivity and piezoresistive properties of these composites and their blends have been reported in a few reports.[44,50–52] However, the investigation of the piezoresistive strain-sensing capacity of PBAT/CNT nanocomposites in detail has not been reported despite their flexibility and ductility. Based on detailed investigations, this study contributes new insights into the strain-induced electromechanical response of biodegradable PBAT/MWCNT nanocomposites with respect to their flexibility and electrical conductivity. The investigation of the strain-sensing potential of CPC fabricated using a flexible and biodegradable polymer matrix will contribute to the goal of sustainable and environment-friendly electronics and sensors to address the global environmental concerns of plastic waste and e-waste.

Materials and methods

Materials

Poly(butylene adipate-*co*-terephthalate) (PBAT) with its trade name Ecoflex® FBX 7011 [molecular weight M_w: 150 000 g mol^{-1}, density: 1.27 g cm^{-3}, elongation at break: >700%, melting temperature: 120 °C, melt mass-flow rate: 4.9 g/10 min (190 °C, 2.16 kg), and glass transition temperature T_g: −30 °C, as presented in the datasheet provided by the manufacturer], a product of BASF, Germany, was used as the polymer matrix. Nanocyl NC7000™ multiwalled carbon nanotubes (MWCNT) [purity: 90%, average diameter: 9.5 nm, and average length: 1.5 μm according to the information in the datasheet provided by the producer], a commercial product of Nanocyl S.A. Company, Belgium, were used as the conductive nanofillers.

Preparation of nanocomposites

MWCNT and granules of PBAT were dried at 120 °C and 80 °C, respectively, for 24 h in a Vacutherm vacuum heating and drying oven (Thermo Fisher Scientific Inc.). MWCNT and PBAT granules were melt-compounded using a twin-screw micro-compounder, Xplore15 (Xplore Instruments BV, Sittard, The Netherlands) at 180 °C with a screw speed of 200 rpm for 5 min with MWCNT concentrations of 0.5, 1, 1.5, 2, 3, 4, 5, 6, and 10 wt%. The composite strands extruded from the micro-compounder were cut into small pieces. These samples were further dried at 80 °C for 24 h under vacuum, from which standard rectangular specimens with a thickness of 0.5 mm, width of 55 mm and length of 80 mm were prepared by compression moulding using a hot press (PW40EH, Otto-Paul-Weber GmbH, Remshalden, Germany) at 180 °C applying 100 kN pressure for 1 min (1.5 min pre-melting time), followed by 5 min cooling. Dumbbell specimens of ISO 527-2 were cut from these rectangular plate specimens applying the force (load) of 1 kN. The prepared nanocomposites were named PBAT/*x*% MWCNT, where *x*% is the weight percentage of MWCNT in the nanocomposites (Table 1).

Characterization techniques

Morphological characterization

Scanning electron microscopy (SEM). A Ultra Plus (Carl Zeiss AG, Oberkochen, Germany) scanning electron microscope in combination with a SE2 detector with a voltage of 3 kV was used for the investigation of the cryofractured surface morphology of the PBAT/MWCNT nanocomposites. The melt-extruded strands of nanocomposites were broken after immersion in liquid nitrogen. The surface of the strands was sputtered with a thin film (thickness: 3 nm) of platinum.

Transmission electron microscopy (TEM). The investigation of the filler dispersion and microstructures of the nanocomposites was carried out employing transmission electron microscopy using a transmission electron microscope (TEM LIBRA-200MC, Carl-Zeiss, Oberkochen, Germany) with an acceleration voltage of 120 kV. Ultra-thin sections (60 nm thick) of PBAT/MWCNT nanocomposites were used for this investigation. Ultra-thin sections were cut perpendicular to the direction of extrusion of the melt-extruded strands using an ultra-microtome EM UB6/FC6 (Leica, Austria) at −160 °C and sectioning speed of 2 mm s^{-1}. Carbon-filmed Cu grids were used for sectioning in dimethyl sulfoxide (DMSO) medium.

Structural characterization. Fourier transform infrared (FTIR) spectroscopy: FTIR spectroscopy was employed to investigate the structure of the nanocomposites and the matrix–filler interaction using a SHIMADZU IRAffinity-1S spectrophotometer in the spectral range of 400–4000 cm^{-1} at the resolution of 10 cm^{-1}.

Electrical characterization

Measurement of electrical volume resistivity. Hot-pressed composite plates and ISO 527-2 standard dumbbell specimens (type S3) cut from the hot-pressed composite plates were measured using a Keithley electrometer E6517A (Keithley Instruments, Solon, USA). For the samples with a volume resistivity of >10^7 Ω cm, the electrometer was combined with a Keithley 8009 (Keithley Instruments, Solon, USA), while for the samples with a volume resistivity of <10^7 Ω cm, it was combined with a 4-point test fixture with gold electrodes having a distance of 10 mm between the electrodes and source electrodes having a distance of 1.6 cm. Two sides of each hot-pressed plate were measured separately and the mean value with standard deviation was calculated. Two sides of each strip cut from the hot-pressed plates using two different strips were measured and the mean value with standard deviation was calculated.

Measurement of piezoresistivity. A Keithley DMM2001 (Keithley Instruments, Solon, USA) electrometer connected to a tensile machine (Zwick/Roell 1456, ZwickRoell GmbH & Co. KG, Ulm, Germany) was used to measure (at 23 °C and 50% humidity) the piezoresistivity of the composites. The tensile machine and electrometer used here could measure strain up to 300% applying the force of 1 kN and resistance of up to 20 GΩ, respectively. Dumbbell specimens of the composites (ISO 527-2 standard according to type S3) cut from the composite plates were fixed in stainless steel clamps at the two heads (clamping distance: 30 mm), while the two ends of the parallel middle part (20 mm long) of the specimens were connected to a DMM2001 (Keithley Instruments, Solon, USA) using clamp wires assuming that elongation occurs at the parallel parts of the specimens during elongation. Silver paste was used at these points for better electrical contact and to reduce the contact resistance between the clamps and the specimens. The electrical

Table 1 List of PBAT/MWCNT nanocomposite samples according to the filler concentration

Sample	PBAT (wt%)
Neat PBAT	100
PBAT/1% MWCNT	99
PBAT/1.5% MWCNT	98.5
PBAT/2% MWCNT	98
PBAT/3% MWCNT	97
PBAT/4% MWCNT	96
PBAT/5% MWCNT	95
PBAT/6% MWCNT	94
PBAT/10% MWCNT	90

resistance (R) was measured as a function of mechanical strain during the experiment. The resistance of each specimen was measured separately using a multi-meter before fixing it in the tensile machine and the value was compared with that at zero tensile strain measured after fixing it in the tensile machine. Both resistance values were found to be nearly the same for all specimens. The specimens were elongated at a cross-head speed of 0.5 mm min^{-1} to record and investigate the minute change in electrical resistance as a function of strain throughout the strain detection range. The tensile machine and the electrometer were clicked at the same time to run them together and the change in the resistance of the samples with an increase in tensile strain and the stress and strain behaviour were simultaneously recorded until sample rupture. The relative resistance change ($\Delta R/R_0$) of the samples was calculated using eqn (1).

$$\Delta R/R_0 = (R - R_0/R_0) \times 100\% \quad (1)$$

where R and R_0 are the resistance of the sample at a certain strain and the resistance at zero strain, respectively. The mechanical strain values were plotted against the $\Delta R/R_0$ values to correlate the change in electrical resistance with the mechanical strain applied. However, the exact information on the elongation of the dumbbell specimens during tensile stretching could not be obtained due to the partial deformation occurring outside their parallel zones. Ultimately, this caused a variation in the gauge factor (GF) of the samples. Similarly, other electrical parameters such as current (I) and voltage (V) were not considered.

Due to this limitation, the time recorded during the electrical resistance measurement was used to correlate the mechanical data with electrical data, instead of calculation of the gauge factor (GF). The piezoresistive sensitivity of the composites was determined considering $\Delta R/R_0$.

Cyclic-strain test. The same set of device combinations used for the measurement of piezoresistivity was used for the cyclic-strain test. The hysteresis test with a cross-head speed of 0.5 mm min^{-1} applying an increasing mechanical strain of 1% to 10% was carried out to identify the strain range with the most reproducible resistance change during strain deformation. Three cyclic measurements for each increasing strain value were carried out with a relaxation time of 90 s for the specimens at the end of each strain loading and unloading in each cycle.

Results and discussion

Morphological and structural characterization of the PBAT/MWCNT nanocomposites

Morphological characterization – scanning electron microscopy (SEM). Scanning electron microscopy (SEM) was employed to assess the distribution of MWCNT in the PBAT/MWCNT nanocomposites (using 1% MWCNT as a concentration close to the percolation threshold), as presented in Fig. 1 on a cryofractured surface.

The SEM micrograph presented in Fig. 1 shows the presence of a uniformly extended rough surface on the nanocomposites.

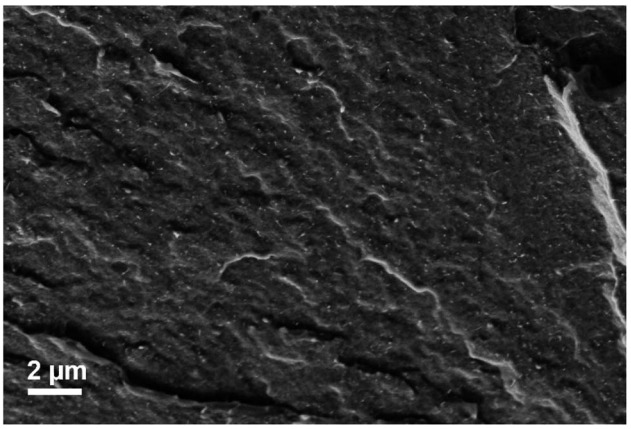

Fig. 1 SEM micrograph of the cryofractured surface of PBAT/1% MWCNT nanocomposites.

It also shows an interconnected MWCNT network throughout the PBAT/MWCNT nanocomposites. A similar surface morphology in PBAT/MWCNT nanocomposites with a higher surface roughness with a higher MWCNT concentration (3 and 10 wt%) was reported in our previous work.[44] However, MWCNT particles, their aggregates and the MWCNT network formed in the nanocomposites could not be detected in these micrographs. For this purpose, transmission electron microscopy (TEM) of the nanocomposites was employed.

Morphological characterization – transmission electron microscopy (TEM). The morphology of the nanocomposites and distribution of MWCNT in the polymer matrix was assessed by transmission electron microscopy (TEM). The TEM micrographs of a thin section of PBAT/MWCNT nanocomposites (using 3% MWCNT to be far from the percolation threshold as an example) under different magnifications are presented in Fig. 2.

The micrographs suggest a uniform distribution of MWCNT particles in the polymer matrix with minor agglomeration. The minor agglomeration of MWCNT in polymer/CNT nanocomposites is reported as a common phenomenon and attributed to the commonly existing van der Waals force of attraction between the CNT particles. It is also ascribed to the flexibility of the PBAT chains and the aromatic ring present in them, leading to a good interfacial matrix–filler interaction. As a result of this interaction, the flexible PBAT chains adsorb onto the surface of MWCNT.[53] The TEM micrograph of the PBAT/3% MWCNT nanocomposite under high magnification clearly shows the evenly embedded individual carbon nanotubes in PBAT. As indicated by the scale bar in the TEM micrograph, the individual carbon nanotubes seem shorter than that mentioned in the Experimental section because it is the cross-sectional view of a thin section of the nanocomposites used in microscopy. The contact between these embedded MWCNT particles eventually results in the formation of an interconnected CNT–CNT network in the nanocomposites. A similar morphology and microstructure in PBAT/MWCNT nanocomposites were reported in the literature.[44,48,54] The uniform distribution of MWCNT in PBAT during melt-mixing with their minor

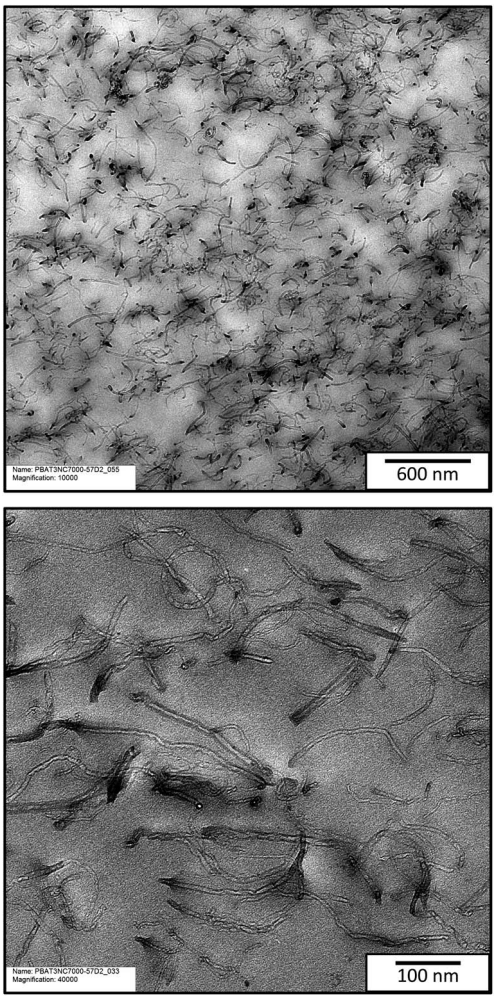

Fig. 2 TEM micrographs of PBAT/3% MWCNT nanocomposites under different magnifications.

agglomeration in the nanocomposites (as suggested by TEM micrographs) can be correlated to the quite low percolation threshold suggested by the volume resistivity values presented in Fig. 4.[44]

Structural characterization – Fourier transform infrared (FTIR) spectroscopy. The FTIR spectra of the neat PBAT and PBAT/3% MWCNT nanocomposites are presented in Fig. 3. The characteristic peaks centred at 724 cm^{-1} and 1455 cm^{-1} are attributed to the –C–H_2 stretching and –C–H_3 bending, respectively, in the PBAT chain.[44,46,55] The peak located at 1713 cm^{-1} corresponds to the C–O stretching vibration, while that at 1269 cm^{-1} corresponds to the carbonyl group (C=O) present in the ester linkage of PBAT.[44,46] Similarly, the peak at 2955 cm^{-1} is associated with the symmetrical –C–H stretching vibration of the aromatic and aliphatic groups[44,56] and the peak at 1501 cm^{-1} corresponds to the aromatic ring of PBAT.[44,50,56]

It seems that the peaks in the spectra of the neat PBAT and composite samples are due to the functional groups and chemical bonds present in PBAT (polymer matrix). No new bands and peak shifting can be observed in the spectrum of the nanocomposites when compared with that of neat PBAT. The exact spectra of the PBAT/MWCNT nanocomposites and neat PBAT imply no chemical interaction between the polymer matrix and fillers. It can be concluded that a physical binding force is responsible for the formation of a nanocomposite microstructure.

Electrical characterization of PBAT/MWCNT nanocomposites

Electrical characterization – volume resistivity. The quantification of electrical conductivity and determination of the electrical percolation threshold were carried out considering the volume resistivity of the PBAT/MWCNT nanocomposites. The addition of MWCNT to the polymer matrix significantly reduced the volume resistivity of the composites. An electrically conductive filler network was formed throughout the polymer matrix at the percolation threshold. It caused an insulator-to-conductor electrical transition in the nanocomposites, transforming them into electrical conductors. The further incorporation of fillers beyond the percolation threshold increased the network density. The volume resistivity of the nanocomposites plotted as a function of MWCNT concentration and the corresponding values are presented in Fig. 4 and Table 2, respectively.

As demonstrated in Table 2, the volume resistivity of the nanocomposites was reduced by several order of magnitude upon the incorporation of 0.5 wt% of fillers, which was further decreased significantly at 1 wt% CNT concentration. The

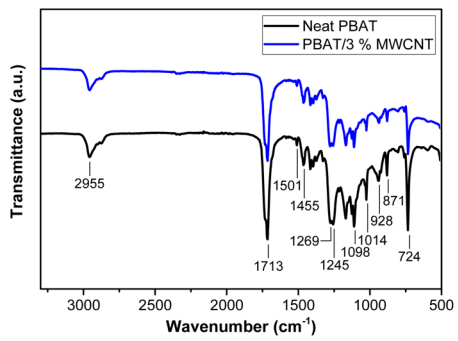

Fig. 3 FTIR spectra of neat PBAT and PBAT/3% MWCNT nanocomposites.

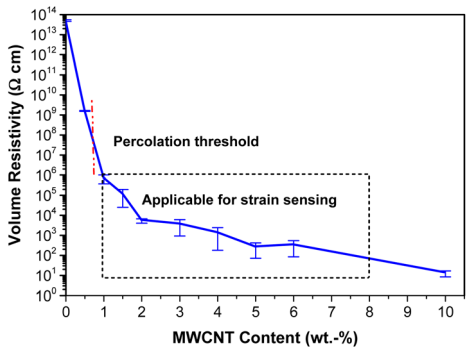

Fig. 4 Electrical volume resistivity of PBAT/MWCNT nanocomposites *versus* MWCNT content.

Table 2 Electrical volume resistivity of neat PBAT and PBAT/MWCNT nanocomposites

Sample	Volume resistivity (Ω cm)
Neat PBAT	$(5.04 \pm 0.44) \times 10^{13}$
PBAT/0.5% MWCNT	$(1.59 \pm 0.09) \times 10^{9}$
PBAT/1% MWCNT	$(6.90 \pm 3.16) \times 10^{5}$
PBAT/1.5% MWCNT	$(1.11 \pm 0.86) \times 10^{5}$
PBAT/2% MWCNT	$(5.36 \pm 1.30) \times 10^{3}$
PBAT/3% MWCNT	$(3.51 \pm 2.58) \times 10^{3}$
PBAT/4% MWCNT	$(1.29 \pm 1.11) \times 10^{3}$
PBAT/5% MWCNT	$(2.49 \pm 1.75) \times 10^{2}$
PBAT/6% MWCNT	$(3.17 \pm 2.32) \times 10^{2}$
PBAT/10% MWCNT	$(1.24 \pm 0.41) \times 10^{1}$

nanocomposites with 0.5 and 1 wt% MWCNT showed volume resistivity values in the range of 10^9 Ω cm and 10^5 Ω cm, respectively. Compared with the reported standard values of volume resistivity of CPC and the classification of electrically conductive materials based on these values, the occurrence of an insulator-to-conductor transition in nanocomposites can be inferred, signifying that the percolation threshold is in the range of 0.5 to 1 wt% MWCNT concentration.[57,58] This implies the formation of a conductive continuous MWCNT network throughout the composites between these two concentrations because the volume resistivity value of the PBAT/1% MWCNT nanocomposite is lower than 10^6 Ω cm, as reported in the literature, which confirms their electrical conductivity.[57–59] The decrease in the volume resistivity of the nanocomposites before the percolation threshold is due to the electron tunnelling effect between the neighbouring CNT particles.[44] The volume resistivity of the nanocomposites continuously decreased with an increase in the filler concentration. When a complete conductive filler-network was formed throughout the nanocomposites at the percolation threshold, the rate of decline in the volume resistivity gradually slowed down at higher filler concentrations. Instead, it only increased the network density in the composites, as suggested by the concentrations beyond 2 wt% of fillers.[60]

A percolation threshold below 1 wt% MWCNT concentration was employed as the low percolation threshold compared to similar works reported in the literature. In similar works, Urquijo *et al.* and Ding *et al.* reported the percolation threshold above 2 wt% of CNT.[49,51] Based on the volume resistivity of the nanocomposites, it seems that the PBAT/0.5% MWCNT nanocomposite is an electrical insulator, whereas PBAT/1% MWCNT and all the other composites with a MWCNT fraction above this concentration are electrically conductive. As suggested by the classification of CPC and their corresponding potential applications based on their volume resistivity values, PBAT/MWCNT nanocomposites at and above the percolation threshold are electrically conductive. The electrical conductivity values of these nanocomposites are sufficient for their potential application as sensors and in electromagnetic interference (EMI) shielding.[57,58] Based on these results, the PBAT/3% MWCNT nanocomposite sample was employed for the investigation of the piezoresistive strain-sensing behaviour, which is discussed in the next section.

This low percolation threshold implies the uniformity in the distribution of MWCNT throughout the nanocomposites.[52] Thus, this confirmed the minor agglomeration of the fillers and their even distribution along with the agglomerates throughout the composite samples. This is an indirect method to correlate the electrical properties of nanocomposites with their morphology considering the state of the filler dispersion.[44] As reported in the literature, a higher percolation threshold would be achieved with a higher agglomeration despite the contribution of the agglomerates to the electrical conductivity, which was not noticed in this work. This type of distribution of filler particles in the nanocomposites with minimum agglomeration supports their integration into strain sensors.[61,62]

Electrical characterization – piezoresistivity. The change in the electrical resistance of the PBAT/MWCNT nanocomposites was measured simultaneously during tensile stretching. Based on the volume resistivity, percolation threshold, filler concentration, *etc.*, the composite sample with 3 wt% of MWCNT was employed for this experiment. A low tensile speed of 0.5 mm min^{-1} was applied for this experiment because the tensile speed affects the range of elastic region of the nanocomposites. In this regard, a higher speed can cause serious damage to the conductive filler network.[63] The inferred ideas garnered from the investigation of minute change in electrical resistance can be supportive to fabricate a CPC-based strain sensor with its tuned performance. The change in electrical resistance as a function of mechanical deformation is expressed in terms of relative resistance change ($\Delta R/R_0$), the magnitude of which is considered to evaluate the strain sensitivity of the nanocomposites.[64] The trend in the change in $\Delta R/R_0$ as a function of tensile strain is presented in Fig. 5a. Similarly, the magnified part of these curves up to 10% strain and 1.6% strain is presented in Fig. 5b and c, respectively. Non-linear and exponentially increasing $\Delta R/R_0$ as a function of mechanical strain confirmed the piezoresistivity of the PBAT/MWCNT nanocomposites.[28,34,65]

The mechanism of the piezoresistive response of the nanocomposites is explained in terms of deformation-induced change in the contact density of the CNT particles, the tunnelling resistance and their microstructures. The increase in the electrical resistance of the nanocomposites during tensile deformation is due to the loss of connections among the MWCNT particles involved in the formation of the conductive network, deformation of individual CNT due to applied strain, increase in tunnelling distance and destruction of the conductive CNT network.[36,66] The interparticle separation between the CNT particles increases during deformation, changing the microstructure of the nanocomposites, and the contact area and degree of electron tunnelling and hopping decrease, leading to an increase in the tunnelling resistance. Similarly, complete disconnection between the filler particles, formation of micro-cracks and their expansion in the nanocomposites occur at higher strain.[19,33,67,68] A low mechanical strain will be sufficient to cause a change in the electrical resistance of the nanocomposites with the filler concentration near the

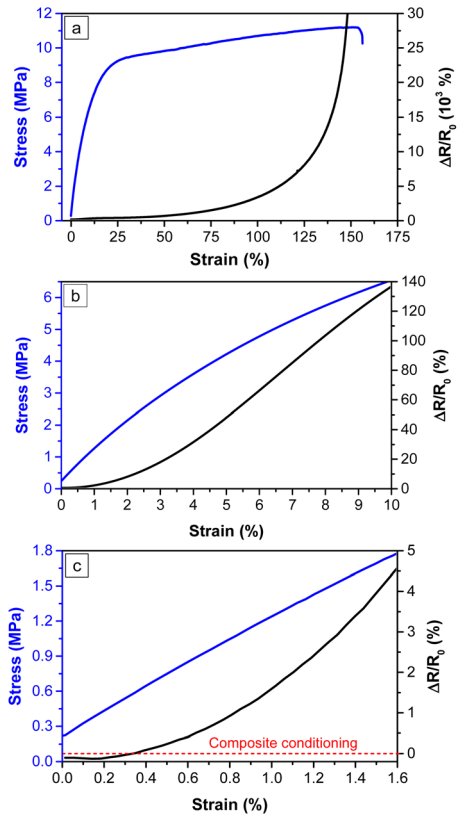

Fig. 5 Stress–strain behaviour and the relative resistance change ($\Delta R/R_0$) of PBAT/3% MWCNT nanocomposites: (a) overview, (b) narrower regime – up to 10% strain, (c) narrowest regime – up to 1.5% strain.

percolation threshold. The nanocomposites are comprised of sparse filler networks, which have the probability of forming alternative conductive paths, contributing to an almost linear piezoresistivity.[1,34,44,68,69] A reversible and temporary breakdown of the CNT network occurs at low-strain level (mostly below the yield point in the elastic region of the thermoplastic-based CPC). As suggested by the stress–strain curves of the PBAT/MWCNT nanocomposites in Fig. 5a, this region is achieved at ~15% strain. Similarly, the abrupt increase in electrical resistance at higher strain is due to the irreversible destruction of the conductive CNT networks due to tensile deformation.[18]

The narrower regime of Fig. 5a, as presented in Fig. 5b, shows the resistance change during measurement up to 10% strain. Similarly, a magnified view (<2% strain) of Fig. 5a is presented in Fig. 5c. The change in electrical resistance as a function of strain follows a quite different trend below 2% strain despite the overall exponential-like manner. Fig. 5c suggests that $\Delta R/R_0$ is negative below 1% strain in comparison to the resistance of the nanocomposites at zero strain (R_0). This strain value is called the critical strain, beyond which the electrical resistance increases exponentially as a function of mechanical strain. Specifically, the negative piezoresistance is changed to positive at critical strain. The breakdown of the conductive network dominates its reconstruction after critical strain. The decrease in resistance below the critical strain is attributed to the composite conditioning, by which the unstable and loose CNT contacts formed by weak filler–matrix interfacial interaction are removed. Moreover, the contact area between the CNT particles increases with a change in the strain, which reduces the electrical resistance.[21] As a consequence, there will be more newly formed CNT–CNT connections at low deformation of the composites, which reduces the electrical resistance.[34,70]

The destruction of the conductive filler network, followed by the simultaneous construction of a new network occurs just beyond the critical strain. These nanocomposites can be applied for low-strain-sensing purposes.[37,68,71] Similarly, higher sensitivity can also be achieved in tunnelling effect-based strain sensors (at lower concentrations); however, their applications are limited due to their poor stretchability and quite complex fabrication processes.[72] Given that the 3 wt% MWCNT nanocomposite used in this test is not so close to the percolation threshold, significant linear piezoresistivity was not observed, as suggested in Fig. 5c. Comparatively, a robust and stable type of filler network should be formed in these nanocomposites, for which a higher strain rate is required to realize piezoresistive sensitivity. Thus, they can be suitable for sensing comparatively higher strain instead of very low strain. The probability of the simultaneous formation of an alternative CNT network decreases at a higher filler concentration.[32,44] Specifically, the piezoresistive sensitivity of CPC can be tuned by altering the conductive filler concentration.

Electrical characterization – strain sensing behaviour. The nanocomposites with the same filler concentration (PBAT/3% MWCNT) used for the investigation of piezoresistivity was also used for the cyclic-strain experiment to investigate its piezoresistive strain sensitivity.

The change in the electrical resistance of the nanocomposites was measured as a function of mechanical strain under cyclic loading/unloading of strain to evaluate its electromechanical response. The $\Delta R/R_0$–strain correlation of the nanocomposites during the cyclic-strain experiment was investigated by measuring its electrical resistance simultaneously with an increased mechanical strain. Mechanical strain was exerted on the nanocomposites in an increasing manner from 1% to 10%, as presented in Fig. 6a–c. The desired strain was exerted on the composite specimen applying the stress followed by a relaxation time of 90 s, after which the applied stress was removed. The same period of relaxation time was provided at the end of each strain unloading. A similar procedure was employed in the experiment up to 10% mechanical strain.

According to Fig. 6a, it can be seen that $\Delta R/R_0$ decreases with mechanical strain up to 1% strain, which is highlighted in Fig. 6c. This result was found to be consistent with that of the uniaxial tensile stretching of the PBAT/3% MWCNT nanocomposite during the investigation of piezoresistivity. Given that the nanocomposite with 3 wt% MWCNT used in this experiment has a filler concentration not close to the percolation threshold, no significant linear piezoresistivity is suggested beyond the critical strain. Instead, it increasingly fitted with mechanical strain, as suggested in Fig. 6b. This result is consistent with that presented in Fig. 5c during the

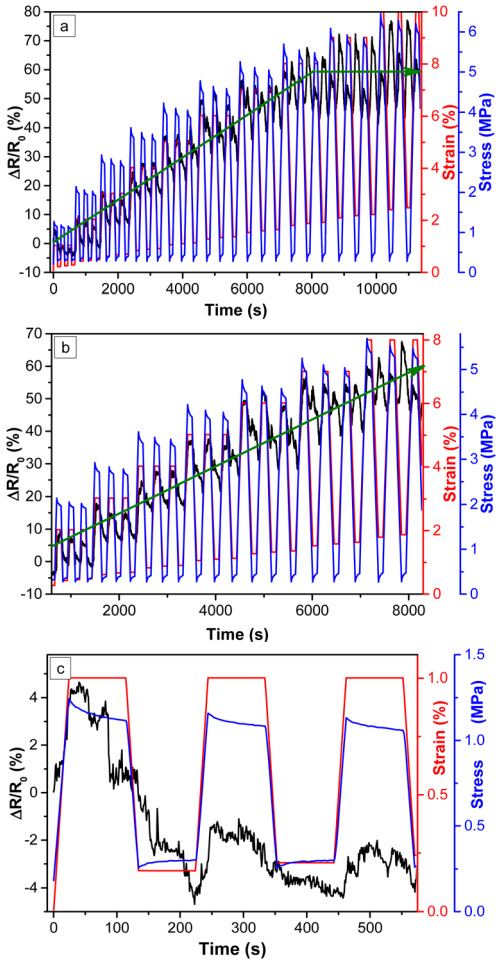

Fig. 6 Cyclic-strain test of PBAT/3% MWCNT nanocomposites with increasing mechanical strain: (a) wide regime (b) closer regime up to 8% strain and (c) closest regime up to 1% strain.

investigation of piezoresistivity. Meanwhile, the $\Delta R/R_0$ values increased with an increase in strain and *vice versa* in each loading and unloading of mechanical stress, respectively, fitting well with the strain from 2% to 8%, as highlighted in Fig. 6b. A positive correlation between $\Delta R/R_0$ and tensile strain is suggested by this experiment, which is a fundamental requirement for CPC to be applied in strain sensors.[63] $\Delta R/R_0$ does not fit well with mechanical strain above 8%, instead it changes in an irregular way regardless the loading and unloading cycles, as shown in Fig. 6a and indicated by the horizontal green arrow. The results of similar works are summarized in Table 3 for a comparison with the results in the current work.

The increase in $\Delta R/R_0$ value as a function of mechanical strain signifies the electromechanical response of the nanocomposites. The increase in the electrical resistance of the nanocomposites upon mechanical strain corresponds to the increase in the tunnelling distance between the filler particles and decrease in the contact between them due to mechanical deformation. Meanwhile, the recovery of the resistance upon removal of the strain is due to the viscoelastic response of the polymer matrix, due to which rearrangement of the deformed filler network takes place during strain unloading. The simultaneous destruction and reconstruction of the filler network coexist during tensile stretching; however, destruction of the network becomes dominant during stretching. Micro-cracks are formed within the matrix–filler network during mechanical loading, due to which the resistance of the nanocomposites increases. These micro-cracks are shrunk and closed during the unloading and relaxation period. Similarly, the strain and amplitude of $\Delta R/R_0$ decrease with time with a reduced tunnelling distance during strain unloading. A certain delay during the recovery of the destroyed network takes place after releasing the mechanical strain.[23,64] The relaxation time provided (90 s in this work) to the nanocomposites after unloading supports $\Delta R/R_0$ to reach the original value by the rearrangement of the deformed CNT network. It also helps to reduce the shoulder peaks. However, resistance overshoots and undershoots also appeared after strain loading and unloading, respectively, which can be more pronounced at higher strain.[73]

A closer view of Fig. 6b suggests that intermediate peaks appear at 4% strain, which become significant and even higher than the first peaks at higher strain (as seen at 8% strain). The first peak corresponds to the resistance change carried out by the maximum strain applied, whereas the second peak is called the shoulder peak. This is a common phenomenon during the deformation of thermoplastic elastomer (TPE)–based conductive nanocomposites. It is due to the competition between the destruction and reconstruction of the new conductive network during the unloading of the strain and viscoplastic property of the polymer matrix. Subsequently, the deformed macromolecular chains of the polymer matrix cannot return to their original position perfectly, causing the formation of shoulder peaks. Competition between the destruction of the old CNT networks and the rearrangement of new paths occurs during strain loading and unloading, respectively.[5,18,24] Furthermore, strain hysteresis occurs during strain unloading, which impedes the rearrangement of the previously destroyed filler network, also leading to the formation of shoulder peaks.[74] During unloading at a higher strain level, residual relative resistance recovery

Table 3 Summary of the strain detection range of different strain sensors

System	Strain range (%)	Reference
Latex tube, core-spun yarn and filter paper with CNTs	0.5–100	1
Latex tube with CNTs	0–200	2
Core-spun yarn, Cu/Al electrodes with LiCl-CNTs	2–100	3
Core-spun yarn with carbon ink	0.5–20	12
PBAT with CNTs	2–8	This work

takes place; however, only a part of the resistance is recovered and the resistance change becomes non-monotonic with the strain. In this way, the recovery of electrical resistance is a time-dependent phenomenon but does not decrease continuously with a decrease in strain. The second peaks appearing between the two successive strain cycles are the negative piezoresistivity, which produce the sensitivity signals in opposite directions and can also be applicable for sensing deformation if recorded accordingly. However, strain sensors based on nanocomposites with dominant first peaks (positive piezoresistivity) are preferred for applications.[18,64] The results summarized in Table 3 imply that the strain detection range of the PBAT/3% MWCNT nanocomposites investigated in this work is low (2% to 8%) in comparison to the strain sensors reported in the literature. Thus, it is concluded that the nanocomposites show low-strain sensing potential and strategic techniques to enhance their strain detection range are recommended.

Given that the strain was set in the experiment and the stress was measured, the resulting stress *vs.* time curve shows the typical viscoelastic effects of stress relaxation. Furthermore, with an increase in strain and time, the residual strain increased, which is related to the change in the CNT–CNT and CNT–matrix interactions (the same behaviour can be seen in Fig. 7).

An additional cyclic-strain test for the PBAT/3% MWCNT nanocomposites was carried out with a higher number of cycles of strain loading/unloading and applying a constant mechanical strain throughout the experiment. The same relaxation time of 90 s after each loading and unloading as that in the previous experiment was applied, where the mechanical strain and number of cycles were different. This cyclic-strain test was targeted to investigate the stability and reproducibility of the piezoresistive sensitivity of the nanocomposites with an increase in the number of cycles. The mechanical strain of 7% was applied in this experiment with 15 loading/unloading cycles. 7% strain was chosen because it is just below the optimum strain range (8%) for the PBAT/3% MWCNT nanocomposites up to which its $\Delta R/R_0$ values fitted well with strain.

The results of the cyclic-strain experiment for the PBAT/3% MWCNT nanocomposite applying 7% strain in 15 cycles are presented in Fig. 7a–c. It seems that the resistance change decayed in the first few cycles (highlighted in Fig. 7b), among which the decay in the first cycle was the most significant. Comparatively, the higher decay of $\Delta R/R_0$ in the first cycle is due to the electromechanical hysteresis of the conductive filler network, due to which the network could not be fully recovered after deformation. This is carried out by mechanical hysteresis of the polymer matrix together with the interfacial interaction between the filler particles and polymer chains at the end of this cycle.[24,32] In successive cycles, the extent of the decay of $\Delta R/R_0$ gradually decreased with an increase in the number of cycles and approached a stable value at higher strain. After several and continuous stretching and releasing cycles, it was stabilized. This is a type of composite conditioning, which is common behaviour in TPE-based nanocomposites and can be explained in accordance with the Mullin's effect. According to the Mullin's effect, the contact surface between filler particles will increase

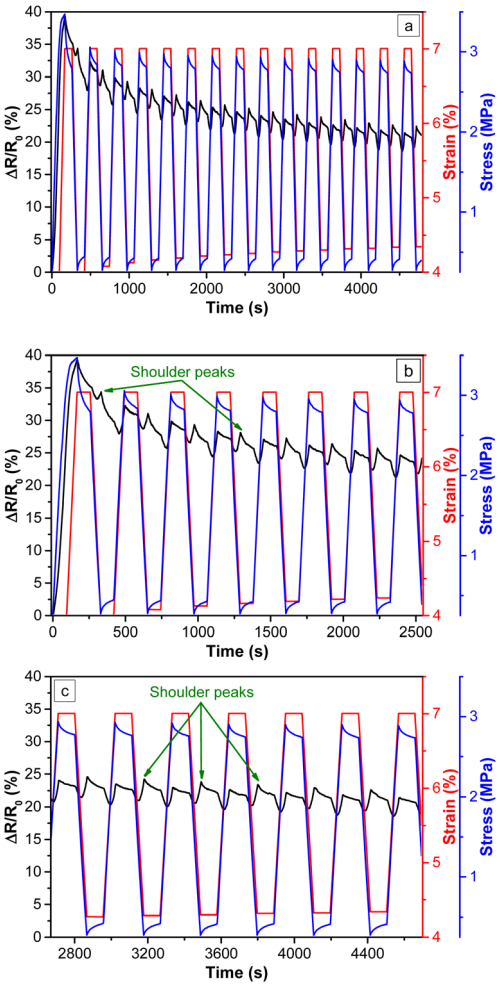

Fig. 7 Cyclic-strain test of PBAT/3% MWCNT nanocomposites with 7% mechanical strain and 15 cycles: (a) wide regime (b) first half of the test and (c) second half of the test.

due to the repeated stretching and releasing of the nanocomposites. There will be decreased and eventually no energy dissipation up on continuous stretching and releasing of the nanocomposites, due to which the nanocomposite microstructure remains intact and stable.[18,64] The polymer chains rearrange themselves at higher strain, which is called strain softening of the polymer matrix. It minimizes the deformation energy and breakage of the polymer chains. After a few cycles, the $\Delta R/R_0$–strain curves reach a plateau at 20%, after which they stabilize and all the resistance amplitudes become almost similar.[62,64,67] These results are consistent with that presented in Fig. 7c. Based on these results and the reports in literature, it can be predicted that the resistance change can be more stabilized beyond 15 cycles.[61,62] If the filler particles are released from the nanocomposites due to weak filler–matrix interfacial interactions, the electrical resistance continuously decreases in successive cycles. Therefore, good interfacial interactions between the fillers and polymer matrix and the stable microstructure after continuous stretching and releasing play a vital role in the piezoresistive strain-sensing behaviour of flexible CPC upon their elastic deformation.[5,75]

The shoulder peaks appearing in this experiment became dominant beyond 4% strain, which is consistent with the results in the previous cyclic-strain test (Fig. 6) for the PBAT/3% MWCNT nanocomposites.

Conclusions

Flexible and electrically conductive PBAT/MWCNT nanocomposites were prepared *via* the incorporation of various concentrations of MWCNT into PBAT by melt-mixing, followed by compression moulding. The decline in the volume resistivity of the nanocomposites with an increase in MWCNT content suggested a percolation threshold lying between 0.5 and 1 wt% of MWCNT. The volume resistivity value of the electrically conductive nanocomposites implied their potential application in strain sensors, as suggested by the volume resistivity-based classification of materials. The piezoresistivity of the nanocomposites was confirmed by their increase in relative resistance change ($\Delta R/R_0$) as a function of strain in a non-linear and exponential-like manner during tensile stretching. Meanwhile, $\Delta R/R_0$ decreased below 1% strain upon tensile stretching, which suggested that this strain is the critical strain. The $\Delta R/R_0$ values of the nanocomposites fitted with the mechanical strain from 2% to 8% in the cyclic-strain test, suggesting their low-strain sensing potential together with shoulder peaks (negative piezoresistivity). This was further supported by the stability and reproducibility of $\Delta R/R_0$ with a higher number of strain loading/unloading cycles and 7% strain. The piezoresistive strain sensing behaviour was provided by the stable and intact microstructure formed by the continuous stretching and releasing of the nanocomposites. An intertwined and entangled filler network with partial agglomeration, formed by the uniformly distributed MWCNT throughout the nanocomposites was revealed by electron micrographs. This work demonstrated that the tuning of the strain-sensing properties of flexible and electrically conductive polymer nanocomposites using biodegradable polymers offers a sustainable strategy for the fabrication of sensors.

Data availability

We hereby confirm that all data related to the research reported in the research article titled 'Piezoresistivity and strain-sensing behaviour of poly(butylene adipate-*co*-terephthalate)/multiwalled carbon nanotube nanocomposites' will be made available.

Author contributions

Conceptualization: RA, formal analysis: KND, funding acquisition: RA, investigation: KND, methodology: KND, BK and JP, project administration: RA, BK and JP, supervision: RA and JP, validation: KND, visualization: KND and RL, writing – original draft: KND, writing – review & editing: RL, WG, BK, JP and RA.

Conflicts of interest

There are no conflicts to declare.

Acknowledgements

Kedar Nath Dhakal gratefully acknowledges Nepal Academy of Science and Technology (NAST) and German Academic Exchange Service (DAAD) for PhD fellowship and funding his research stay in Germany, respectively. Ulrike Jentzsch-Hutschenreuther (for sample preparation), and Holger Scheibner (for tensile test and cyclic-strain tests) from Leibniz-Institut für Polymerforschung (IPF) Dresden e. V., Germany are sincerely thanked. Similarly, Petr Formanek and Uta Reuter from IPF are gratefully thanked for TEM microscopy. RA thanks the Alexander von Humboldt (AvH) Foundation, Germany for supporting his research stays at IPF, Dresden (2016), and PSM, Merseburg (2023).

References

1 Q. Huang, Y. Jiang, Z. Duan, Y. Wu, Z. Yuan, M. Zhang and H. Tai, *Chem. Eng. J.*, 2024, **490**, 151660.
2 Z. Yuan, H. Li, Z. Duan, Q. Huang, M. Zhang, H. Zhang, J. Guo, Y. Jiang and H. Tai, *Sens. Actuators, A*, 2024, **369**, 115202.
3 Q. Huang, Y. Jiang, Z. Duan, Y. Wu, Z. Yuan, M. Zhang, Q. Zhao, Y. Zhang, B. Liu and H. Tai, *Nano Energy*, 2023, **118**, 108997.
4 Y. Zhang, J. Xu and H. Wang, *RSC Adv.*, 2021, **11**, 37661–37666.
5 H. Gong, C. Cai, H. Gu, Q. Jiang, D. Zhang and Z. Cheng, *RSC Adv.*, 2021, **11**, 4186–4193.
6 E. Caffrey, J. M. Munuera, T. Carey and J. N. Coleman, *Nanoscale Horiz.*, 2024, **9**, 1774–1784.
7 X. Wang, H. Li, T. Wang, X. Niu, Y. Wang, S. Xu, Y. Jiang, L. Chen and H. Liu, *RSC Adv.*, 2022, **12**, 14190–14196.
8 R. A. Qazi, M. S. Khan, L. A. Shah, R. Ullah, A. Kausar and R. Khattak, *Polym.-Plast. Technol. Mater.*, 2020, **59**, 928–951.
9 K. S. Kim, J. Yoo, J. S. Shim, Y. I. Ryu, S. Choi, J. Y. Lee, H. M. Lee, J. Koo and S. K. Kang, *Adv. Mater. Technol.*, 2022, **7**, 1–12.
10 Y. Guo, X. Zuo, Y. Xue, J. Tang, M. Gouzman, Y. Fang, Y. Zhou, L. Wang, Y. Yu and M. H. Rafailovich, *Composites, Part B*, 2020, **189**, 107905.
11 A. P. B. Silva, L. S. Montagna, F. R. Passador, M. C. Rezende and A. P. Lemes, *eXPRESS Polym. Lett.*, 2021, **15**, 987–1003.
12 Z. Duan, Y. Jiang, S. Wang, Z. Yuan, Q. Zhao, G. Xie, X. Du and H. Tai, *ACS Sustain. Chem. Eng.*, 2019, **7**, 17474–17481.
13 D. Moraru, A. Cort, D. Martinez-diaz, S. G. Prolongo, A. Jim and M. Sangermano, *polymers*, 2024, **16**, 1–11.
14 K. Qian, J. Zhou, M. Miao, H. Wu, S. Thaiboonrod, J. Fang and X. Feng, *Nano-Micro Lett.*, 2023, **15**, 1–18.
15 J. Yang, H. Wang, Y. Zhang, H. Zhang and J. Gu, *Nano-Micro Lett.*, 2024, **16**, 1–14.
16 W. B. Han, S. M. Yang, K. Rajaram and S. W. Hwang, *Adv. Sustainable Syst.*, 2022, **6**, 1–17.

17 H. Wang, X. Yu, X. Tang, Y. Sun, X. Zeng and L. Lin, *Cellulose*, 2022, **29**, 341–354.
18 S. Salaeh, A. Das, K. W. Stöckelhuber and S. Wießner, *Composites, Part A*, 2020, **130**, 105763.
19 A. Leber, S. Laperrousaz, Y. Qu, C. Dong, I. Richard and F. Sorin, *Adv. Sci.*, 2023, **10**, 1–11.
20 T. Li, Z. Duan, Q. Huang, H. Yang, Z. Yuan, Y. Jiang and H. Tai, *Sens. Actuators, A*, 2024, **376**, 115629.
21 X. Feng, Y. Ran, X. Li, H. Xu, Q. Huang, Z. Duan, Z. Yuan, Y. Jiang and H. Tai, *Mater. Chem. Phys.*, 2024, **321**, 129489.
22 Q. Huang, Y. Jiang, Z. Duan, Z. Yuan, Y. Wu, J. Peng, Y. Xu, H. Li, H. He and H. Tai, *IEEE Sens. J.*, 2023, **23**, 13789–13796.
23 Z. Wang, Y. Cong and J. Fu, *J. Mater. Chem. B*, 2020, **8**, 3437–3459.
24 C. Mastropasqua, A. Veca, A. Damin, V. Brunella and F. Cesano, *Nanomaterials*, 2022, **13**, 168.
25 J. Cob, A. I. Oliva-Avilés, F. Avilés and A. I. Oliva, *Mater. Res. Express*, 2019, **6**, 115024.
26 S. H. Hwang, H. W. Park and Y. Bin Park, *Smart Mater. Struct.*, 2013, **22**, 015013.
27 Y. F. Liu, W. Wang and X. F. Chen, *Front. Bioeng. Biotechnol.*, 2023, **11**, 1–15.
28 K. Ke, P. Pötschke, S. Gao and B. Voit, *ACS Appl. Mater. Interfaces*, 2017, **9**, 5437–5446.
29 K. Gao, Z. Zhang, S. Weng, H. Zhu, H. Yu and T. Peng, *Appl. Sci.*, 2022, **12**, 9750.
30 S. Han, H. Tan, J. Wei, H. Yuan, S. Li, P. Yang, H. Mi, C. Liu and C. Shen, *Adv. Sci.*, 2023, **10**, 2301713.
31 Z. Wang and X. Ye, *Nanotechnology*, 2014, **25**, 285502.
32 X. Wang, S. Meng, M. Tebyetekerwa, Y. Li, J. Pionteck, B. Sun, Z. Qin and M. Zhu, *Composites, Part A*, 2018, **105**, 291–299.
33 X. L. Xu, S. X. Li, Y. Yang, X. C. Sun and H. Xia, *Measurement*, 2022, **189**, 110658.
34 X. Tang, P. Pötschke, J. Pionteck, Y. Li, P. Formanek and B. Voit, *ACS Appl. Mater. Interfaces*, 2020, **12**, 43125–43137.
35 C. Wang, X. Li, E. L. Gao, M. Q. Jian, K. L. Xia, Q. Wang, Z. P. Xu, T. L. Ren and Y. Y. Zhang, *Adv. Mater.*, 2016, **28**, 6640–6648.
36 M. Amjadi, Y. J. Yoon and I. Park, *Nanotechnology*, 2015, **26**, 375501.
37 P. Costa, J. Nunes-Pereira, J. Oliveira, J. Silva, J. A. Moreira, S. A. C. Carabineiro, J. G. Buijnsters and S. Lanceros-Mendez, *Compos. Sci. Technol.*, 2017, **153**, 241–252.
38 A. Georgopoulou, S. Srisawadi, P. Wiroonpochit and F. Clemens, *Polymers*, 2023, **15**, 2410.
39 M. J. Yee, N. M. Mubarak, E. C. Abdullah, M. Khalid, R. Walvekar, R. R. Karri, S. Nizamuddin and A. Numan, *Nano-Struct. Nano-Objects*, 2019, **18**, 100312.
40 F. Avilés, A. May-Pat, M. A. López-Manchado, R. Verdejo, A. Bachmatiuk and M. H. Rümmeli, *Eur. Polym. J.*, 2018, **99**, 394–402.
41 Y. Lin, S. Liu, S. Chen, Y. Wei, X. Dong and L. Liu, *J. Mater. Chem. C*, 2016, **4**, 6345–6352.
42 X. G. Yu, Y. Q. Li, W. Bin Zhu, P. Huang, T. T. Wang, N. Hu and S. Y. Fu, *Nanoscale*, 2017, **9**, 6680–6685.
43 M. M. Reddy, S. Vivekanandhan, M. Misra, S. K. Bhatia and A. K. Mohanty, *Prog. Polym. Sci.*, 2013, **38**, 1653–1689.
44 K. N. Dhakal, S. Khanal, B. Krause, R. Lach, W. Grellmann, H. H. Le, A. Das, S. Wießner, G. Heinrich, J. Pionteck and R. Adhikari, *Nano-Struct. Nano-Objects*, 2022, **29**, 100806.
45 N. L. Bhandari, S. Thomas, C. K. Das and R. Adhikari, *J. Nepal Chem. Soc.*, 2013, **29**, 113–120.
46 S. Pokhrel, A. Sigdel, R. Lach, M. Slouf, J. Sirc, V. Katiyar, D. R. Bhattarai and R. Adhikari, *J. Macromol. Sci., Part A: Pure Appl.Chem.*, 2021, **58**, 610–621.
47 J. Giri, R. Lach, H. H. Le, W. Grellmann, J. M. Saiter, S. Henning, H. J. Radusch and R. Adhikari, *Polym. Bull.*, 2021, **78**, 4779–4795.
48 S. Y. Hong, S. W. Ko, H. J. Choi and J. H. Lee, *J. Macromol. Sci., Part B: Phys.*, 2012, **51**, 125–133.
49 K. Ding, N. Wei, Y. Zhou, Y. Wang, D. Wu, H. Liu, H. Yu, C. Zhou, J. Chen and C. Chen, *J. Compos. Mater.*, 2016, **50**, 1805–1816.
50 K. N. Dhakal, B. Krause, R. Lach, A. Wutzler, W. Grellmann, H. H. Le, A. Das, S. Wießner, G. Heinrich and R. Adhikari, *J. Appl. Polym. Sci.*, 2022, **139**, 1–12.
51 J. Urquijo, N. Aranburu, S. Dagréou, G. Guerrica-Echevarría and J. I. Eguiazábal, *Eur. Polym. J.*, 2017, **93**, 545–555.
52 E. J. Dil, M. Arjmand, I. O. Navas, U. Sundararaj and B. D. Favis, *Macromolecules*, 2020, **53**, 10267–10277.
53 R. Zhang, H. Deng, R. Valenca, J. Jin, Q. Fu, E. Bilotti and T. Peijs, *Compos. Sci. Technol.*, 2013, **74**, 1–5.
54 S. W. Ko, M. K. Hong, B. J. Park, R. K. Gupta, H. J. Choi and S. N. Bhattacharya, *Polym. Bull.*, 2009, **63**, 125–134.
55 A. M. Díez-Pascual and A. L. Díez-Vicente, *RSC Adv.*, 2015, **5**, 93095–93107.
56 M. Zhang, Y. Zhang, Q. Liu, W. Q. He and J. Liu, *RSC Adv.*, 2024, **14**, 3611–3616.
57 H. Pang, L. Xu, D. X. Yan and Z. M. Li, *Prog. Polym. Sci.*, 2014, **39**, 1908–1933.
58 G. Kaur, R. Adhikari, P. Cass, M. Bown and P. Gunatillake, *RSC Adv.*, 2015, **5**, 37553–37567.
59 B. Krause, P. Pötschke, E. Ilin and M. Predtechenskiy, *Polymer*, 2016, **98**, 45–50.
60 J. F. Christ, N. Aliheidari, A. Ameli and P. Pötschke, *Mater. Des.*, 2017, **131**, 394–401.
61 Z. Sang, K. Ke and I. Manas-Zloczower, *Composites, Part A*, 2019, **121**, 207–212.
62 D. Xiang, X. Zhang, Y. Li, E. Harkin-Jones, Y. Zheng, L. Wang, C. Zhao and P. Wang, *Composites, Part B*, 2019, **176**, 107250.
63 P. Li, Y. Xia, C. Zhang, C. Wang, Y. Liu, H. Fang and F. Wang, *J. Mater. Res. Technol.*, 2024, **28**, 2127–2137.
64 A. Moshkriz, Z. Shahroodi and R. Darvishi, *RSC Adv.*, 2023, **13**, 17818–17833.
65 D. G. Papageorgiou, Z. Li, M. Liu, I. A. Kinloch and R. J. Young, *Nanoscale*, 2020, **12**, 2228–2267.
66 M. Amjadi, A. Pichitpajongkit, S. Lee, S. Ryu and I. Park, *ACS Nano*, 2014, **8**, 5154–5163.
67 B. Wan, Y. Yang, R. Guo, Z. Fan, P. Deng and S. Zhang, *Polymers*, 2023, **15**, 1412.
68 D. D. L. Chung, *J. Mater. Sci.*, 2020, **55**, 15367–15396.

69 H. Liu, M. Dong, W. Huang, J. Gao, K. Dai, J. Guo, G. Zheng, C. Liu, C. Shen and Z. Guo, *J. Mater. Chem. C*, 2017, **5**, 73–83.
70 M. Ji, H. Deng, D. Yan, X. Li, L. Duan and Q. Fu, *Compos. Sci. Technol.*, 2014, **92**, 16–26.
71 X. Liao, Z. Zhang, Z. Kang, F. Gao, Q. Liao and Y. Zhang, *Mater. Horiz.*, 2017, **4**, 502–510.
72 Y. Tang, Z. Zhao, H. Hu, Y. Liu, X. Wang, S. Zhou and J. Qiu, *ACS Appl. Mater. Interfaces*, 2015, **7**, 27432–27439.
73 A. Georgopoulou and F. Clemens, *ACS Appl. Electron. Mater.*, 2020, **2**, 1826–1842.
74 X. Liu, R. Guo, Z. Lin, Y. Yang, H. Xia and Z. Yao, *Nanomater. Nanotechnol.*, 2021, **11**, 1–13.
75 S. Wu, J. Zhang, R. B. Ladani, A. R. Ravindran, A. P. Mouritz, A. J. Kinloch and C. H. Wang, *ACS Appl. Mater. Interfaces*, 2017, **9**, 14207–14215.